PAPER

Check for updates

Two-dimensional superconducting nature of Bi₂Sr₂CaCu₂O₈₊δ thin films revealed by BKT transition

Liping Zhang, [a] Chaoyang Kang,[a] Chengyan Liu, [a] Kai Wang*[b] and Weifeng Zhang*[ac]

High-quality Bi₂Sr₂CaCu₂O₈₊δ superconducting thin films are successfully grown on a SrTiO₃ substrate by the Pulsed Laser Deposition technique. Superconducting critical transition temperatures $T_{c,zero}$ have reached up to 85 K by using optimized growth parameters. In addition, we demonstrated the two-dimensional nature of the superconductivity of thin films by virtue of exhibiting Berezinskii–Kosterlitz–Thouless (BKT) physics and anisotropic magnetic response. Furthermore, three distinct regimes are identified based on the analysis of direct current resistance. The non-Fermi liquid phase and BKT phase fluctuation zone almost perfectly merge together, which implies that the system undergoes a unique topological state that is determined by the BKT phase fluctuation preceding the onset of the superconducting state. The emergence of such a topological state radically differentiates from the three-dimensional superconducting transition, which spontaneously breaks the gauge symmetry. The current studies on the Bi₂Sr₂CaCu₂O₈₊δ superconducting thin films provide some new insights for understanding the rich quantum states of matter that emerge in the vicinity of the superconducting phase transition and highlight the significant role of BKT fluctuation on two-dimensional superconducting transition.

1. Introduction

Studies on high-temperature superconductivity have attracted substantial attention due to their fascinating macro quantum phenomenon and elusive superconducting pair mechanisms.[1–3] In particular, various two-dimensional (2D) materials and heterostructures have been considered to be promising platforms for establishing high-temperature superconductivity in the past several decades.[4–7] For example, 2D materials MoS₂ and ZrNCl exhibit a superconducting critical transition temperature T_c which is comparable with their bulk counterparts.[8–16] The La₂₋ₓSrₓCuO₄/La₂CuO₄ heterostructure interfaces and FeSe thin films even display a transition temperature much higher than the bulk values.[17–22] In particular, the LaAlO₃/KTaO₃ interface shows superconductivity whereas their bulk forms are both not superconductors.[23] The representative works demonstrate that 2D superconducting phase transition could be different from the case of 3D. 2D-related materials and other artificial structures give us a new platform to realize high-temperature

superconductivity and explore the superconducting physical origin.

In addition, owing to the development of the mechanical exfoliation technique, Yu *et al.* successfully realize the fabrication of intrinsic monolayer crystals of the high-temperature superconductors Bi₂Sr₂CaCu₂O₈₊δ (Bi-2212). The oxygen content of monolayer Bi-2212 can be tuned by annealing. The investigations on the superconductivity, pseudogap phenomenon, charge density wave order, and Mott insulating states of monolayer Bi-2212 at different doping concentrations both turn out to be consistent with the observations in the bulk phase. These important discoveries demonstrate that cuprate superconductors are characteristic of quasi-two-dimensional.[24] However, although the preparation of monolayer high-temperature superconductors can be achieved through mechanical exfoliation techniques, there are huge challenges in practical applications due to the small size and uncontrollable thickness. Therefore, we prepared superconducting thin films of Bi-2212 by using the Pulsed Laser Deposition (PLD) technique. The size is relatively larger and the thickness of the film can be controlled, which enables the application of superconducting thin films to become possible. The Bi-2212 thin films grown on SrTiO₃ substrate exhibit the highest superconducting transition temperature. The growth parameters, such as laser energy density, oxygen partial pressure and deposition temperature, are optimized to obtain a relatively

[a]School of Future Technology, Henan University, Zhengzhou 450046, China. E-mail: wfzhang@henu.edu.cn

[b]Center for Topological Functional Materials, Henan University, Kaifeng 475004, China. E-mail: kai.wang@henu.edu.cn

[c]Institute of Quantum Materials and Physics, Henan Academy of Sciences, Zhengzhou 450046, China

high transition temperature, which reaches up to 85 K by using optimal growth conditions. In addition to that, the application of a magnetic field leads to the suppression of high-temperature superconductivity. Especially for the application of an out-of-plane magnetic field, the critical transition temperature was remarkably changed. The linear fitting extrapolating of the critical magnetic field at 0 K reaches 52.77 T, which is a comparable energy size with the corresponding critical temperature. Finally, we employ the Berezinskii–Kosterlitz–Thouless (BKT) formula to fit the direct current (DC) resistance. We found that the low-temperature resistance can be well fit by the BKT phase fluctuation formula ahead of the superconducting state, which signifies the characteristics of 2D superconductivity. In the high-temperature region, the mysterious linear temperature-dependent behavior has been recognized as the signature of Non-Fermi liquid states, which remains to be elusive so far. In this paper, we highlight two important facts, one is that three distinct regimes can be distinguished only through the analysis of DC resistance. Another point is that the emergence of a topological state caused by BKT phase fluctuation is a key difference in contrast with the 3D superconductivity. In other words, 2D superconducting phase transition does not require the spontaneous symmetry breaking due to the existence of the topological state.

2. Experiment methods and measurements

Thin films of Bi-2212 are prepared on single crystalline substrates of $SrTiO_3$ (STO), $LaAlO_3$ (LAO) and $DyScO_3$ (DSO) by using the pulsed laser deposition (PLD) technique with a Coherent KrF Excimer laser of wavelength 248 nm. The target of nominal composition Bi-2212 is prepared by the solid-state reaction method. The metal carbonates used for the synthesis were dried prior to the reactions and the drying temperatures is 200 °C. The raw materials (Bi_2O_3, $SrCO_3$, $CaCO_3$ and CuO) are weighed according to stoichiometric ratio, thoroughly ground in an agate mortar to obtain a homogeneous mixture, and then calcined at 760 °C for 10 hours to remove carbonate. The calcined powder is fully ground again and calcined at 830 °C for 10 hours. This process needs to be repeated several times until the pure powder phase of Bi-2212 is obtained, which is placed in the vacuum hot-pressing furnace for the final pressing and sintering process. The XRD pattern of Bi-2212 polycrystalline target is shown in Fig. 1(a). The film deposition parameters are optimized by varying the laser energy density, oxygen partial pressure, substrate temperature and *in situ* annealing conditions. The high-quality superconducting Bi-2212 thin films are obtained by the use of the best deposition parameters. Before
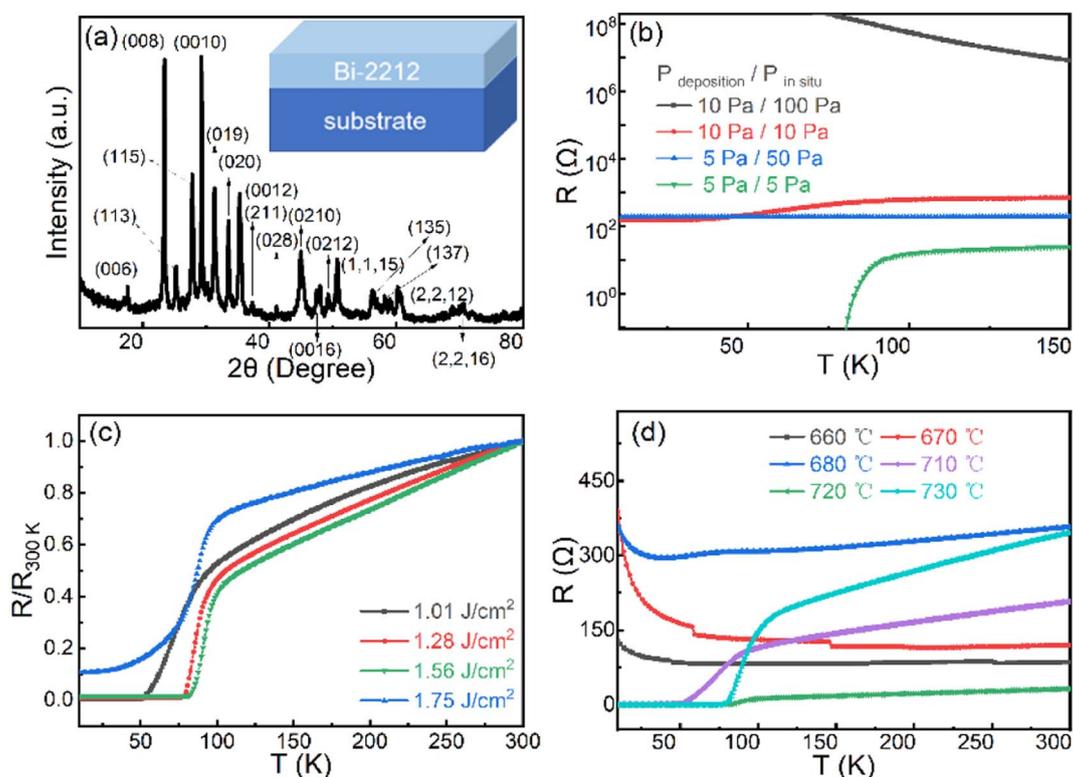
Fig. 1 The fabrication of the superconducting Bi-2212 thin film device. (a) XRD pattern of the polycrystalline Bi-2212 and schematic diagram of Bi-2212 thin film structure. (b) The temperature dependence of DC resistance is shown in different colors, which represents the growth condition of the thin film in different combinations of deposition O_2 pressure and *in situ* annealing O_2 pressure respectively. (c) Likewise, renormalized resistance of the Bi-2212 thin film device is present in different laser energy densities. Obviously, the laser energy density has an important impact on the superconducting phase transition temperature T_c. (d) The temperature dependence of DC resistance is shown in different $SrTiO_3$ substrate temperatures.

each deposition, the chamber is evacuated to a base pressure of 2.64×10^{-6} Pa and the deposition frequency is set at 2 Hz. The substrate-to-target distance is fixed at 9.3 cm. To optimize the growing conditions, the laser energy density is varied from 1.01 J cm^{-2} to 1.75 J cm^{-2}, the deposition pressure from 5 Pa to 10 Pa O_2, the substrate temperature from 660 °C to 730 °C, and the O_2 pressure *in situ* annealing varies from 5 Pa to 100 Pa. *In situ* annealing is used to improve the crystallinity of the samples, and the pieces are kept warm for 20 minutes before the deposition to clean the substrate. Magneto transport measurements are performed using the commercial 9 T magnetoresistance setup from Quantum Design, US. The magnetic field can be applied in the direction of both parallel and perpendicular to the plane of the sample in the temperature range from 1.9 K to 400 K. The maximum value of the magnetic field can reach 9 T. The high-resolution X-ray diffraction (HR-XRD, $\lambda = 1.5406$ Å, Bruker D8 advance) patterns of the films are measured in the θ–2θ mode at room temperature. The surface morphology of the Bi-2212 thin film is characterized by atomic force microscopy (AFM, Bruker MultiMode 8).

3. Results and discussion

By analyzing the influence of deposition parameters on transporting property of the superconducting thin films, the preparation technology of thin films is optimized to obtain the Bi-2212 thin film devices which perform the clear superconducting phase transition. Firstly, Bi-2212 thin films are deposited on the STO substrates by fixing the laser energy density at 1.56 J cm^{-2} and the substrate temperature at 720 °C, and then one tried to use different combinations of deposition O_2 pressure and in situ annealing O_2 pressure to obtain the best-deposited parameters. Fig. 1(b) shows the temperature dependence of DC resistance ($R(T)$) of Bi-2212 films in different growth conditions. The black (red/blue/green) curve represents the Bi-2212 film deposited at 10 (10/5/5) Pa O_2 pressure and annealed *in situ* at 100 (10/50/5) Pa O_2 pressure. We find that the film grown at 5 Pa O_2 pressure and annealed at 5 Pa O_2 pressure exhibits a sharp superconducting phase transition, and other combinations of deposition O_2 pressure and *in situ* annealing O_2 pressure show a metallic behavior or an insulating behavior. Apparently, the transporting property of the Bi-2212 thin films is sensitive to O_2 pressure, which gives rise to insulator-metal-superconductor phase transition through controlling O element concentrations of $Bi_2Sr_2CaCu_2O_{8+\delta}$. This change in transporting behavior makes us reminiscent of hole-doping driving insulator-superconducting-metal phase transition in cuprate superconductors.[25] The black curve can correspond to the underdoped sample, where a typical Mott insulating behavior emerges. The red and blue curves show a metallic behavior, which can be understood as the consequence of being over-doped.

As shown in Fig. 1(c) and (d), the laser energy density and substrate temperature both have a significant influence on the superconducting phase transition of the Bi-2212 thin film. The
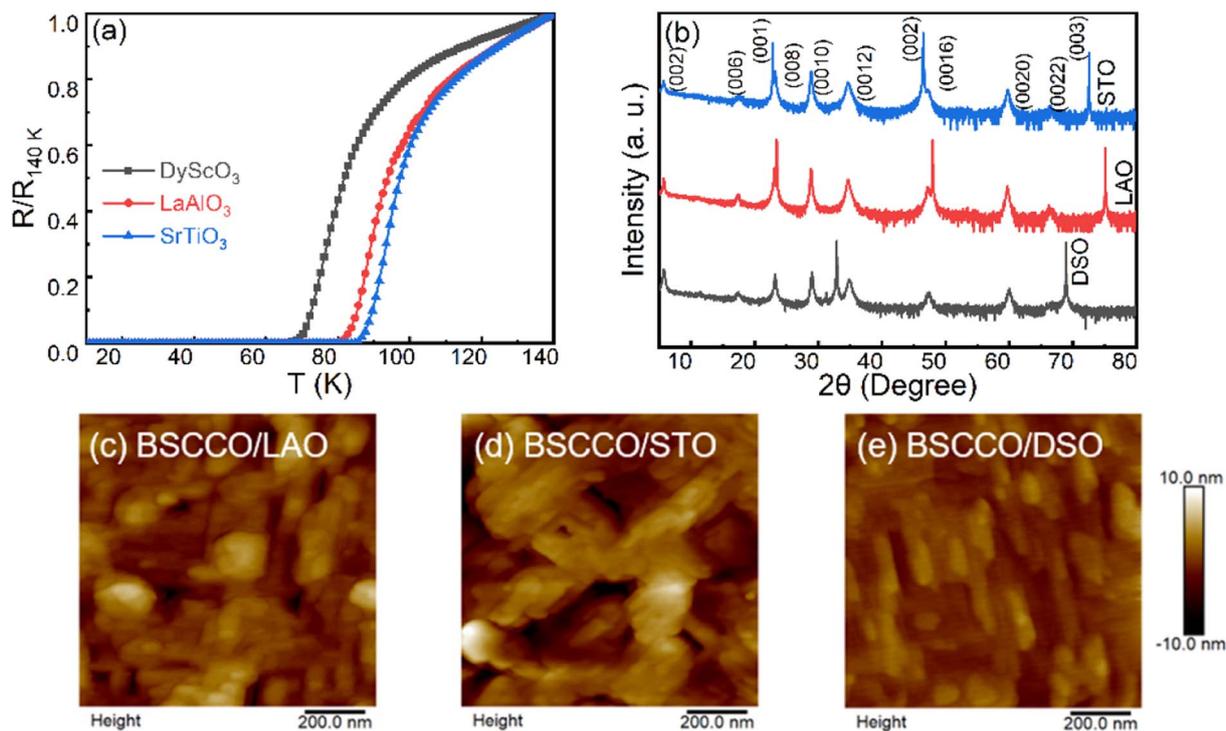

Fig. 2 X-ray diffraction (XRD) and atomic force microscopy (AFM) for Bi-2212 thin film device. (a) Renormalized resistance of Bi-2212 thin film grown in different substrates is displayed. As we can see, Bi-2212 thin film with SrTiO$_3$ substrate demonstrates the highest superconducting phase transition temperature T_c. (b) The high-resolution X-ray diffraction patterns of Bi-2212 films deposited on SrTiO$_3$, LaAlO$_3$, and DyScO$_3$ substrates are measured in the θ–2θ mode respectively. (c–e) The surface topography images of the films deposited on SrTiO$_3$, LaAlO$_3$ and DyScO$_3$ substrates are shown respectively.

best laser energy density and substrate temperature that we obtain through the data of Fig. 1(c) and (d) are around 1.56 J cm^{-2} and 720 °C, respectively. For the laser energy density, a larger one than 1.56 J cm^{-2} generates a bigger size of Bi-2212 grains, which will lead to the partial isolation of these grains from the substrates, thereby weakening the superconductivity. Likewise, the substrate temperature also should not be too high, which also can cause the isolation of the film from the substrates.[26] In addition to that, in order to obtain the best performance of superconducting thin films, we try to select three different substrates in which all compounds possess a perovskite crystal structure. Thus, these high-quality superconducting thin films are allowed to be deposited in our selected substrates due to their small lattice mismatch with the cuprate lattice. As shown in Fig. 2(a), the three devices of Bi-2212/STO, Bi-2212/LAO and Bi-2212/DSO all exhibit a sharp superconducting phase transition, thereinto, the STO device demonstrates the highest superconducting transition temperature. To analyze the underlying relationship between lattice mismatches and superconducting phase transition, one calculated the lattice mismatch degrees for all the devices by the formula $(a_s - a_t)/a_s$, where a_s is the lattice parameter of the substrate and a_t is the lattice parameter of the Bi-2212 phase. Then we obtained the values of +2.05%, −0.92% and +3.85% on STO, LAO, and DSO respectively. However, the size of lattice mismatch degrees does not be proportional or inverse to the

superconducting phase transition temperature, which indicates that the determination of superconducting critical phase transition temperature is complex, and the lattice mismatch degrees could only induce a negligible effect. A plausible explanation is that the degrees of lattice mismatch can not directly determine the numbers of the surface defect and O element concentration, which change the superconducting phase transition. The high-resolution X-ray diffraction patterns of Bi-2212 films deposited on STO, LAO, and DSO substrate are measured in the θ–2θ mode, respectively, shown in Fig. 2(b), where the $(00l)$ diffraction peaks from the Bi-2212 thin film and STO, LAO and DSO substrate are clearly observed. The presence of the $(002l)$ peak confirms the c-axis orientation of the Bi-2212 thin film, which implies the current studied thin film is a high-quality single crystal thin film.

$$2d \sin \theta = n\lambda \tag{1}$$

$$d = \frac{1}{\sqrt{\dfrac{h^2 + K^2}{a^2} + \dfrac{l^2}{c^2}}} \tag{2}$$

According to the Bragg derivative formula of (1) and the interplanar spacing formula of the tetragonal crystal system of (2), the c-lattice parameter of the Bi-2212 film deposited on the STO, LAO and DSO substrates are determined from the XRD
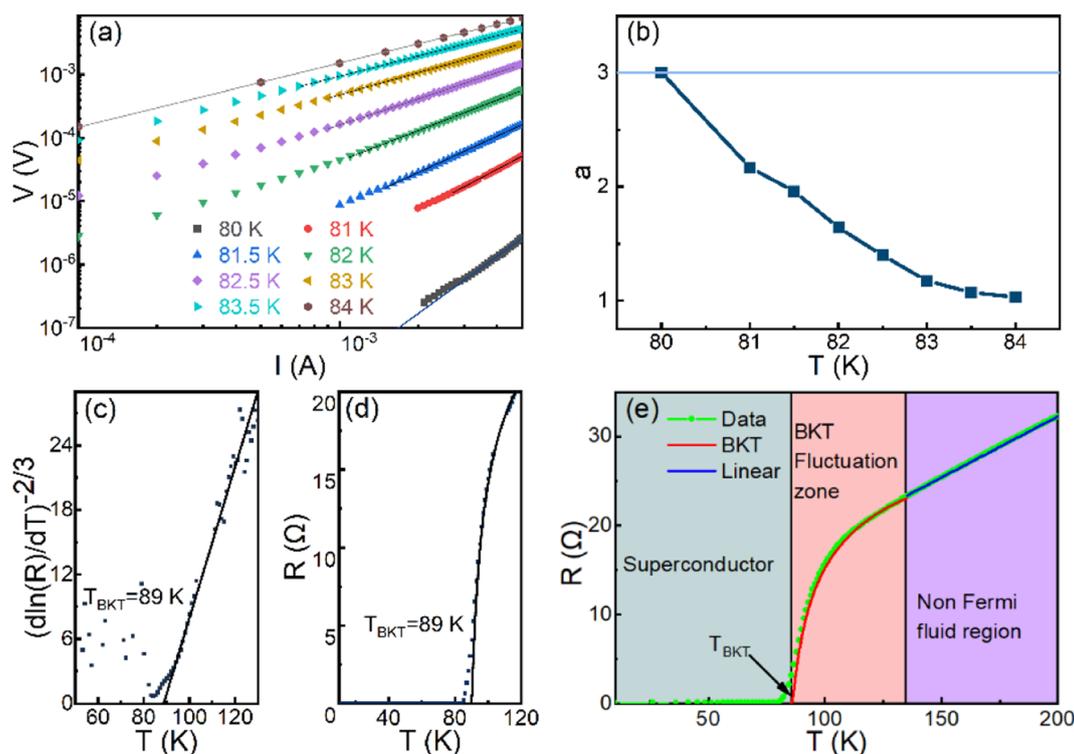

Fig. 3 The analysis of BKT transition. (a) $V(I)$ curves on a logarithmic scale for Bi-2212 thin film device. (b) The temperature dependence of the power-law exponent is shown, which comes from the fits for $V(I)$ curves in (a). (c) $R(T)$ dependence plotted on a $[\text{d} \ln T/\text{d}(T)]^{-2/3}$ versus T scale. The solid line denotes the behavior that is expected for a BKT transition with $T_{\text{BKT}} = 89$ K. (d) $R(T)$ is directly fit by using the BKT formula, yielding a $T_{\text{BKT}} = 89$ K. (e) The phase diagram is summarized based on our measured DC resistance for the thin film device. The red and blue solid lines indicate the BKT fit and linear fit in different temperature ranges respectively.

(002l) diffraction peak, which was 30.691 Å, 30.785 Å and 30.5 Å. The atomic force microscope measurement shows that the surface of Bi-2212/STO, Bi-2212/LAO and Bi-2212/DSO are quite flat with a roughness of about 2.57, 1.86 and 1.89 nm in Fig. 2(c)–(e). Loosely speaking, XRD patterns and AFM images both indicate that the high-quality superconducting thin films are already grown in different substrates.

By investigating the transport properties of the Bi-2212/STO heterostructure and observing whether it has the characteristics of the BKT transition or not, which can determine whether the observed superconductivity has a 2D nature? For 2D systems, the superconducting phase transition should exhibit a BKT transition which is characterized by a transition temperature T_{BKT}.[27–32] Vortex–antivortex pairs are formed below T_{BKT}, and the zero-resistance state appears. As the temperature increases, vortex–antivortex pairs bonded at low temperatures can spontaneously unbind into free vortices above T_{BKT} due to thermodynamic instability, and eventually, the superconducting state is destroyed through the proliferation of free vortices at a higher temperature.[33]

According to the BKT transition theory, two typical signatures can be identified in the vicinity of the characteristic transition temperature T_{BKT}, (I) the non-ohmic behavior of V–I curve appears as a simple power-law behavior $V \propto I^{a(T)}$ with $a = 3$ at T_{BKT};[28,31,34,35] and (II) the temperature dependence of the resistance manifests as $R(T) = R_0 e^{-b(T-T_{BKT})-1/2}$,[28,32] which can be equivalently to write a logarithmic form as $[d \ln T/d(T)]^{-2/3} = 2/b^{2/3}(T - T_{BKT})$, i.e., the expression $[d \ln T/d(T)]^{-2/3}$ possess a linear temperature dependence. These two features have been currently used to experimentally confirm the existence of a BKT transition and determine the value of the T_{BKT}.[6,32–37] Fig. 3(a) displays the V–I curves (log–log scale) for the sample. The straight lines in this figure imply the power-law behavior, and the power law exponents a is equal to the slope of the lines ($V \propto I^a$). Among them, the grey line with a slope of 1 which indicates their ohmic characteristics of normal state resistance ($V \propto I$), while the blue line with slope 3 marks the beginning of the BKT transition ($V \propto I^3$). The power-law exponents as a function temperature are extracted by the fit for V–I curves at each temperature. As shown in Fig. 3(b), the value of a is close to 3 at a temperature of 80 K, hence T_{BKT} is estimated to be 80 K by V–I characteristics. In addition, the R(T) characteristics should also be consistent with the BKT transition. As expected for the BKT transition (see (II) above), $[d \ln T/d(T)]^{-2/3}$ around T_{BKT} should be linear with T. As shown by the blue line in Fig. 3(c), $[d \ln T/d(T)]^{-2/3}$ does scale linearly with T. $T_{BKT} = 89$ K that is extracted from the intersection point of the linear extrapolation with the X axis.[6,32] At the
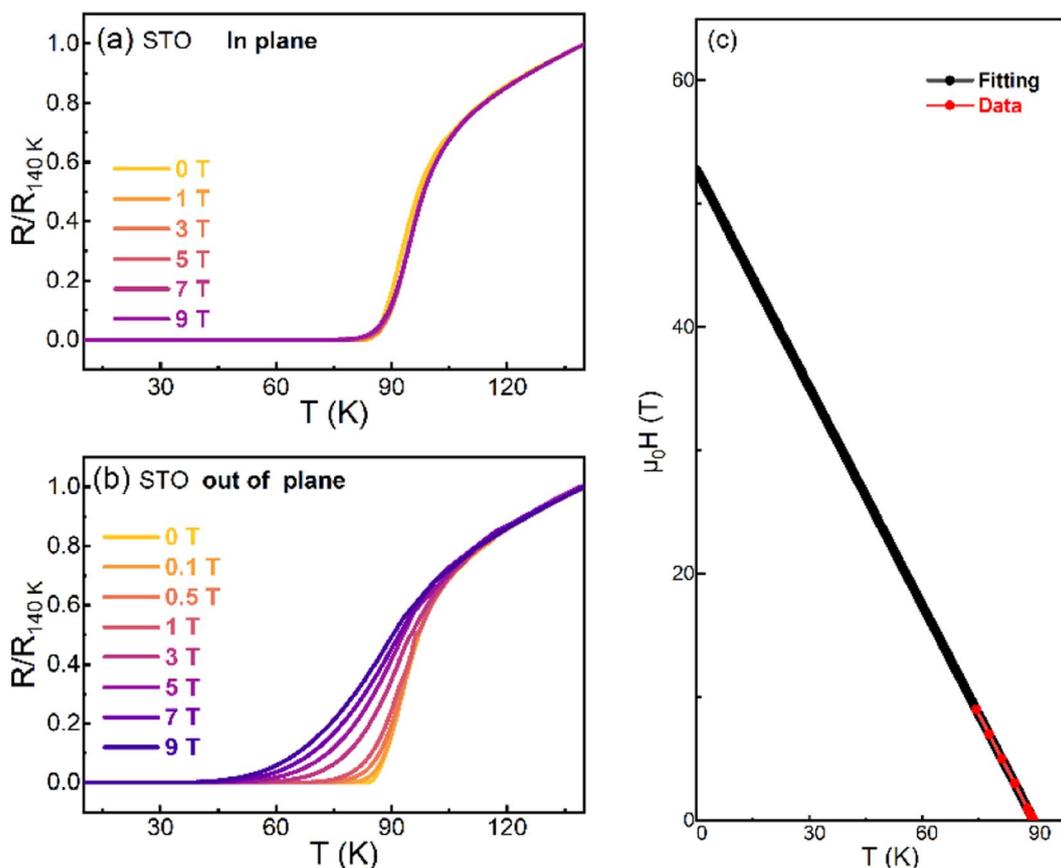

Fig. 4 Anisotropic magnetic response of Bi-2212 thin film device. (a) The normalized resistance of the film deposited on the SrTiO₃ substrate is plotted as a function of temperature with the application of an in-plane magnetic field. (b) The normalized resistance of the Bi-2212 thin film device is shown under the out-of-plane magnetic field. (c) According to (b), the temperature dependence of the critical magnetic field in the out-of-plane direction is fit. The application of an out-of-plane magnetic field of 52.77 T can totally suppress the superconductivity.

temperature range just above T_{BKT}, the temperature-dependent resistance is predicted to be in a form of $R(T) = R_0 \, e^{-b(T-T_{BKT})-1/2}$, where R_0 and b are material-specific parameters.[6,28,38–40] The plot of $[d \ln T/d(T)]^{-2/3}$ versus T as shown in Fig. 3(c) and the fits using this form of the $R(T)$ data shown in Fig. 3(d) are both in accordance with the expectation of BKT transition theory, yielding T_{BKT} to be 89 K. As we discussed above, T_{BKT} that deduced from the V–I characteristic and $R(T)$ curve is quite close.

Furthermore, the phase diagram is summarized based on our measured DC resistance for the thin film device in Fig. 3(e). The blue curve is obtained by a linear fitting, the fitting formula is $R(T) = 0.138T + 4.68$. The red curve is obtained by BKT fitting, the fitting formula is $R(T) = R_0 \, e^{-b(T-T_{BKT})-1/2}$. Intriguingly, the BKT fit and linear fit can be clearly distinguished, and these two fitting lines almost seamlessly merge together. This implies that the system has to undergo a BKT phase fluctuation region as a transition state ahead of the emergence of the superconducting state. This is intrinsically distinct from the appearance of 3D bulk superconductivity. In addition, at higher temperature ranges, we also observe the linear temperature dependence which has already been thought of as the typical feature of non-Fermi liquid states, however, its physical origin is still elusive so far. Around the BKT temperature, the absolute zero resistance state has a tiny deviation from the BKT formula, which means that the finite size effect and inhomogeneity of the thin films have a weak impact on the superconducting transition.[41]

Magneto transport measurements are performed on the optimized thin film grown on the STO substrate. Fig. 4(a) and (b) correspond to the magnetic transport measurements of the film under an in-plane and out-of-plane magnetic field respectively. The resistance $R(T)$ has been normalized to that of 140 K. The superconductivity of this heterostructure sample cannot be fully destroyed by applying magnetic fields up to 9 T out of a plane or in the plane, which implies their upper critical fields ($\mu_0 H$) are quite large. In contrast with the response of in the plane magnetic field, the superconductivity is remarkably suppressed under the magnetic field out of the plane, which also reflects the feature of 2D superconductivity. $R(T)$ curves at different magnetic fields of out of plane are fitted by using the BKT formula as $R(T) = R_0 \, e^{-b(T-T_{BKT})-1/2}$. The magnetic fields are found to be linear as a function of BKT transition temperature (see Fig. 4(c)). By using the formula $\mu_0 H(T_{BKT}) = -0.58T_{BKT} + 52.77$ to fit the data, the critical magnetic field at zero temperature can be determined, which is about 52.77 T. The corresponding Zeeman energy is 6.1 meV, which is about 70 K, which is a bit lower than the critical superconducting transition temperature.

4. Conclusions

In summary, firstly, the high-quality $Bi_2Sr_2CaCu_2O_{8+\delta}$ superconducting thin films are successfully grown on various substrates by the PLD technique. Different O_2 pressure leads to qualitatively different transporting behavior and displays an insulator-superconductor-metal phase transition, which can be attributed to the change in O concentrations. Superconducting critical transition temperature has reached up to 85 K by using the optimized growth parameters on the STO substrate. Lattice mismatch cannot determine the superconducting phase transition. Secondly, the BKT formula is employed to well fit the DC resistance. The BKT characteristic temperature determined by V–I curves and $R(T)$ date are quite close, which confirms the 2D superconducting nature of thin films. Finally, the BKT fit and linear fit are well distinguished, and three distinct phases (superconducting phase, BKT phase fluctuation state, non-Fermi liquid state) are identified only through DC resistance. Our current work on $Bi_2Sr_2CaCu_2O_{8+\delta}$ superconducting thin films provides some new insights for understanding the 2D superconducting phase transition and highlights the significant role of BKT phase fluctuation.

Conflicts of interest

There are conflicts to declare.

Acknowledgements

References

1 B. Keimer, S. A. Kivelson, M. R. Norman, S. Uchida and J. Zaanen, *Nature*, 2015, **518**, 179–186.

2 C. Song, X. Ma and Q. Xue, *Sci. Sin.*, 2021, **51**, 1–28.

3 V. N. Kotov, O. P. Sushkov, M. B. Silva Neto, L. Benfatto and A. H. Castro Neto, *Phys. Rev. B: Condens. Matter Mater. Phys.*, 2007, **76**, 1–5.

4 M. Johannes, I. Mazin and C. Howells, *Phys. Rev. B: Condens. Matter Mater. Phys.*, 2006, **73**, 1–8.

5 D. Shaffer, J. Kang, F. J. Burnell and R. M. Fernandes, *Phys. Rev. B*, 2020, **101**, 1–16.

6 N. Reyren, S. Thiel, A. D. Caviglia, L. F. Kourkoutis, G. Hammerl, C. Richter, C. W. Schneider, T. Kopp, A. S. Ruetschi, D. Jaccard, M. Gabay, D. A. Muller, J. M. Triscone and J. Mannhart, *Science*, 2007, **317**, 1196–1199.

7 J. Biscaras, N. Bergeal, A. Kushwaha, T. Wolf, A. Rastogi, R. C. Budhani and J. Lesueur, *Nat. Commun.*, 2010, **1**, 1–5.

8 Y. Saito, Y. Nakamura, M. S. Bahramy, Y. Kohama, J. Ye, Y. Kasahara, Y. Nakagawa, M. Onga, M. Tokunaga, T. Nojima, Y. Yanase and Y. Iwasa, *Nat. Phys.*, 2015, **12**, 144–149.

9 J. M. Lu, O. Zheliuk, I. Leermakers, N. F. Q. Yuan, U. Zeitler, K. T. Law and J. T. Ye, *Science*, 2015, **350**, 1353–1357.

10 J. T. Ye, Y. J. Zhang, R. Akashi, M. S. Bahramy, R. Arita and Y. Iwasa, *Science*, 2012, **338**, 1193–1196.

11 J. T. Ye, S. Inoue, K. Kobayashi, Y. Kasahara, H. T. Yuan, H. Shimotani and Y. Iwasa, *Nat. Mater.*, 2010, **9**, 125–128.

12 Y. Saito, Y. Kasahara, J. Ye, Y. Iwasa and T. Nojima, *Science*, 2015, **350**, 409–413.

13 S. Yamanaka, H. Kawaji, K.-i. Hotehama and M. Ohashi, *Adv. Mater.*, 1996, **8**, 771–774.

14 T. Ito, Y. Fudamoto, A. Fukaya, I. M. Gat-Malureanu, M. I. Larkin, P. L. Russo, A. Savici, Y. J. Uemura, K. Groves, R. Breslow, K. Hotehama, S. Yamanaka, P. Kyriakou, M. Rovers, G. M. Luke and K. M. Kojima, *Phys. Rev. B: Condens. Matter Mater. Phys.*, 2004, **69**, 1–13.

15 Y. Taguchi, A. Kitora and Y. Iwasa, *Phys. Rev. Lett.*, 2006, **97**, 1–4.

16 T. Takano, A. Kitora, Y. Taguchi and Y. Iwasa, *Phys. Rev. B: Condens. Matter Mater. Phys.*, 2008, **77**, 1–6.

17 A. Gozar, G. Logvenov, L. F. Kourkoutis, A. T. Bollinger, L. A. Giannuzzi, D. A. Muller and I. Bozovic, *Nature*, 2008, **455**, 782–785.

18 J. Wu, O. Pelleg, G. Logvenov, A. T. Bollinger, Y. J. Sun, G. S. Boebinger, M. Vanevic, Z. Radovic and I. Bozovic, *Nat. Mater.*, 2013, **12**, 877–881.

19 X. Shi, P. V. Lin, T. Sasagawa, V. Dobrosavljević and D. Popović, *Nat. Phys.*, 2014, **10**, 437–443.

20 Q.-Y. Wang, Z. Li, W.-H. Zhang, Z.-C. Zhang, J.-S. Zhang, W. Li, H. Ding, Y.-B. Ou, P. Deng, K. Chang, J. Wen, C.-L. Song, K. He, J.-F. Jia, S.-H. Ji, Y.-Y. Wang, L.-L. Wang, X. Chen, X.-C. Ma and Q.-K. Xue, *Chin. Phys. Lett.*, 2012, **29**, 1–4.

21 F. C. Hsu, J. Y. Luo, K. W. Yeh, T. K. Chen, T. W. Huang, P. M. Wu, Y. C. Lee, Y. L. Huang, Y. Y. Chu, D. C. Yan and M. K. Wu, *Proc. Natl. Acad. Sci. USA*, 2008, **105**, 14262–14264.

22 J. F. Ge, Z. L. Liu, C. Liu, C. L. Gao, D. Qian, Q. K. Xue, Y. Liu and J. F. Jia, *Nat. Mater.*, 2015, **14**, 285–289.

23 Z. Chen, Y. Liu, H. Zhang, Z. Liu, H. Tian, Y. Sun, M. Zhang, Y. Zhou, J. Sun and Y. Xie, *Science*, 2021, **372**, 721–724.

24 Y. Yu, L. Ma, P. Cai, R. Zhong, C. Ye, J. Shen, G. D. Gu, X. H. Chen and Y. Zhang, *Nature*, 2019, **575**, 156–163.

25 E. Sterpetti, J. Biscaras, A. Erb and A. Shukla, *Nat. Commun.*, 2017, **8**, 2060.

26 G. V. S. Bera, E. P. Amaladass, T. G. Kumary, R. Pandian and A. Mani, *Phys. Chem. Chem. Phys.*, 2021, **23**, 12822–12833.

27 M. R. Beasley, J. E. Mooij and T. P. Orlando, *Phys. Rev. Lett.*, 1979, **42**, 1165–1168.

28 B. I. Halperin and D. R. Nelson, *J. Low Temp. Phys.*, 1979, **36**, 599–616.

29 Z. Ovadyahu, *Phys. Rev. Lett.*, 1980, **45**, 375–378.

30 N. A. H. K. Rao, E. D. Dahlberg, A. M. Goldman, L. E. Toth and C. Umbach, *Phys. Rev. Lett.*, 1980, **44**, 98–102.

31 K. Epstein, A. M. Goldman and A. M. Kadin, *Phys. Rev. Lett.*, 1981, **47**, 534–537.

32 J.-H. She and A. V. Balatsky, *Phys. Rev. Lett.*, 2012, **109**, 1–5.

33 S. Weyeneth, T. Schneider and E. Giannini, *Phys. Rev. B: Condens. Matter Mater. Phys.*, 2009, **79**, 1–8.

34 D. J. Resnick, J. C. Garland, J. T. Boyd, S. Shoemaker and R. S. Newrock, *Phys. Rev. Lett.*, 1981, **47**, 1542–1545.

35 D. W. Abraham, C. J. Lobb, M. Tinkham and T. M. Klapwijk, *Phy. Rev. B*, 1982, **26**, 5268–5271.

36 N. Cotón, M. V. Ramallo and F. Vidal, *Supercond. Sci. Technol.*, 2011, **24**, 1–8.

37 A. M. Kadin, K. Epstein and A. M. Goldman, *Phys. Rev. B: Condens. Matter Mater. Phys.*, 1983, **27**, 6691–6702.

38 J. M. Kosterlitz, *Phys. Status Solidi C*, 1974, **7**, 1046–1060.

39 O. Yuli, I. Asulin, O. Millo, D. Orgad, L. Iomin and G. Koren, *Phys. Rev. Lett.*, 2008, **101**, 1–4.

40 J. M. Kosterlitz and D. J. Thouless, *J. Phys. C Solid State Phys.*, 1973, **6**, 1181–1203.

41 L. Benfatto, C. Castellani and T. Giamarchi, *Phys. Rev. B: Condens. Matter Mater. Phys.*, 2009, **80**, 1–11.